Emission-wavelength tuning of InAs quantum dots grown on nitrogen-δ-doped GaAs(001)

Kaizu, Toshiyuki
Taguchi, Kohei
Kita, Takashi

(Citation)
Journal of Applied Physics,119(19):194306-194306

(Issue Date)
2016-05-21

(Resource Type)
journal article

(Version)
Version of Record

AIP Journal of Applied Physics

Emission-wavelength tuning of InAs quantum dots grown on nitrogen-δ-doped GaAs(001)

Toshiyuki Kaizu, Kohei Taguchi, and Takashi Kita

Citation: Journal of Applied Physics **119**, 194306 (2016); doi: 10.1063/1.4951719
View online: http://dx.doi.org/10.1063/1.4951719
View Table of Contents: http://scitation.aip.org/content/aip/journal/jap/119/19?ver=pdfcov
Published by the AIP Publishing

Emission-wavelength tuning of InAs quantum dots grown on nitrogen-δ-doped GaAs(001)

Toshiyuki Kaizu,[1,2,a)] Kohei Taguchi,[2] and Takashi Kita[2]
[1]*Center for Supports to Research and Education Activities, Kobe University, 1-1 Rokkodai, Nada, Kobe 657-8501, Japan*
[2]*Department of Electrical and Electronic Engineering, Faculty of Engineering, Kobe University, 1-1 Rokkodai, Nada, Kobe 657-8501, Japan*

(Received 9 March 2016; accepted 10 May 2016; published online 20 May 2016)

We studied the structural and photoluminescence (PL) characteristics of InAs quantum dots (QDs) grown on nitrogen (N) δ-doped GaAs(001). The emission wavelength for low-density N-δ doping exhibited a blueshift with respect to that for undoped GaAs and was redshifted with increasing N-sheet density. This behavior corresponded to the variation in the In composition of the QDs. N-δ doping has two opposite and competing effects on the incorporation of Ga atoms from the underlying layer into the QDs during the QD growth. One is the enhancement of Ga incorporation induced by the lattice strain, which is due to the smaller radius of N atoms. The other is an effect blocking for Ga incorporation, which is due to the large bonding energy of Ga-N or In-N. At a low N-sheet density, the lattice-strain effect was dominant, while the blocking effect became larger with increasing N-sheet density. Therefore, the incorporation of Ga from the underlying layer depended on the N-sheet density. Since the In-Ga intermixing between the QDs and the GaAs cap layer during capping also depended on the size of the as-grown QDs, which was affected by the N-sheet density, the superposition of these three factors determined the composition of the QDs. In addition, the piezoelectric effect, which was induced with increased accumulation of lattice strain and the associated high In composition, also affected the PL properties of the QDs. As a result, tuning of the emission wavelength from 1.12 to 1.26 μm was achieved at room temperature. *Published by AIP Publishing.* [http://dx.doi.org/10.1063/1.4951719]

I. INTRODUCTION

Self-assembled InAs quantum dots (QDs) are a promising material for advanced optical communication devices such as cooler-free low-power-consumption lasers[1–3] and polarization-insensitive semiconductor optical amplifiers (SOAs).[4–9] These devices are required to operate not only in the optical communication bands of 1.3 and 1.55 μm but also in the shorter bands of 1.0 to 1.3 μm expected to be used in the future expansion of optical networking. To achieve a broader operational bandwidth, control of the emission wavelengths of QDs is important. The emission wavelength of QDs is significantly affected by the size of the as-grown QDs and the variation in size during GaAs capping. Various methods have been demonstrated for controlling the size of as-grown and embedded QDs: adjustment of the QD growth conditions,[10] the introduction of an InGaAs strain-reducing layer,[11,12] and In flushing.[13,14] Another factor that affects the emission wavelength is the composition of the QDs. Ga atoms are incorporated into QDs owing to intermixing between the QDs and the GaAs matrix not only during GaAs capping[15,16] but also during QD growth.[17–19] The In-Ga intermixing between the QDs and the GaAs cap layer is also accompanied by QD shrinkage, and thereby, the emission wavelength of the QDs is blueshifted.[20] Several methods have been demonstrated for controlling the intermixing during capping, such as adjustment of the capping temperature[21] and the doping of a nitrogen (N) layer (called N-δ doping) on the QD surface.[22–24] In contrast, the incorporation of Ga atoms from the underlying layer induces an increase in the QD size,[25] which depends on the QD growth conditions. Since the emission wavelength of the QDs is determined by the competition between the effects of the dot size and the composition, its tunable bandwidth due to the QD growth conditions is restricted.

In this paper, we propose a method for controlling the photoluminescence (PL) emission wavelength by growing InAs QDs on a N-δ-doped GaAs. Such N-δ doping was performed in an atomically controlled way using the N-stabilized surface on GaAs(001),[26,27] in which the active N species were supplied to the GaAs surface. The QDs grown on low-density N-δ-doped GaAs exhibited a blueshifted emission with respect to those grown on undoped GaAs, and the emission wavelength was redshifted with increasing N-sheet density. As a result, tuning of the emission wavelength from 1.12 to 1.26 μm was achieved at room temperature. Furthermore, we analyzed the QD morphology after capping, the temperature dependence of the PL, and the PL decay times for various N-sheet densities, and we discuss the mechanism of the shift in the emission wavelength.

II. EXPERIMENTAL PROCEDURE

The samples were grown on semi-insulating GaAs(001) substrates using a solid-source molecular beam epitaxy apparatus equipped with a radio-frequency (rf) plasma source.

a)Electronic mail: kaizu@crystal.kobe-u.ac.jp

After the removal of the oxide layer at 585 °C, a 400-nm-thick GaAs buffer layer was deposited at 550 °C. Then, the substrate temperature, which was monitored using an infrared pyrometer, was lowered to 480 °C. N-δ doping was performed after confirming the c(4 × 4) reconstructed surface under an As_2-beam-equivalent pressure of 1.3×10^{-3} Pa, in which the active N species created using the plasma source from ultrapure N_2 gas were supplied to the GaAs surface. The N partial pressure was 1.7×10^{-3} Pa, and the gas-flow rate was 0.35 ccm. The rf power was set at 440 W. Reflection high-energy electron diffraction (RHEED) patterns obtained from the [-110] azimuth before and after N-δ doping are shown in Figs. 1(a) and 1(b), respectively. The c(4 × 4) streak pattern gradually changed to the (3 × 3) pattern during N-δ doping. This indicates that a N-stabilized reconstructed surface is formed by the substitution of N atoms for As atoms.[26,27] The N-sheet densities were estimated from the N-irradiation time dependence of the N-sheet density. The N-sheet densities (n_s), which were derived from the secondary ion mass spectroscopy (SIMS) profile shown in the inset, are plotted as a function of the N-irradiation time (t) in Fig. 1(c). Since n_s is almost proportional to t, we can control n_s precisely. In this study, n_s was varied from 0.85×10^{12} to 34×10^{12} cm^{-2}. After the rf power was turned off, the growth was interrupted for 120 s, which was equivalent to the growth interruption introduced in the SIMS sample. InAs QDs with a nominal thickness of 2.0 monolayers (ML) were grown by self-assembly, and subsequently, a 100-nm-thick GaAs cap layer was deposited. The growth rates of InAs and GaAs were 0.04 and 0.8 ML/s, respectively.

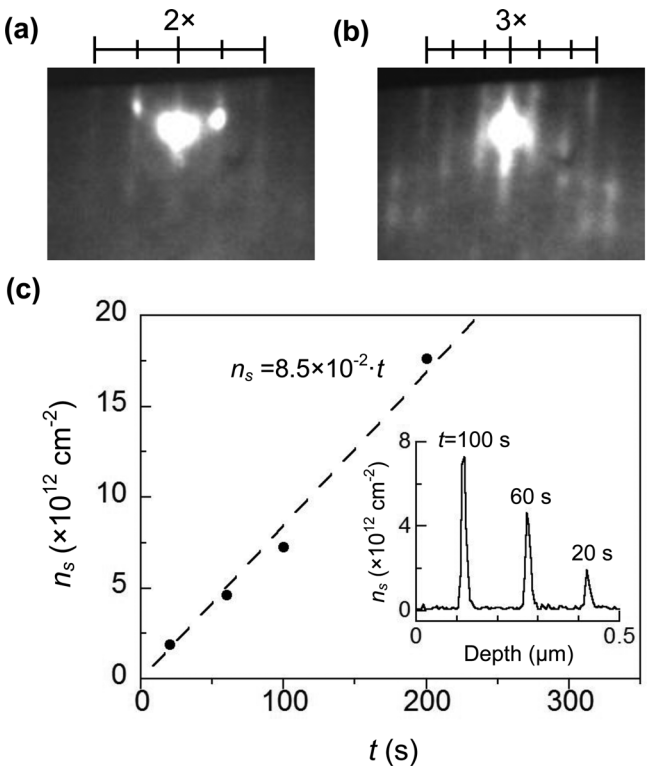

FIG. 1. RHEED patterns observed from the [-110] azimuth (a) before and (b) after N-δ doping. (c) N-sheet densities (n_s) analyzed by SIMS as a function of the N-irradiation time (t). The inset shows the SIMS profile of the N-δ-doped sample with various N-sheet densities. The broken line denotes the linear dependence of n_s on t.

The morphology of the as-grown and embedded QDs was analyzed by atomic force microscopy (AFM) in the contact mode and cross-sectional high-angle annular dark-field scanning transmission electron microscopy (HAADF-STEM), respectively. PL measurements were performed using a continuous-wave laser diode with a wavelength of 659 nm. The excitation power was 15 mW. The PL signal was dispersed using a 30 cm single monochromator and detected using a liquid-nitrogen-cooled InGaAs diode array. In addition, time-resolved PL measurements were performed using a near-infrared streak camera system with a temporal resolution of 20 ps. The light source used was a mode-locked Ti:sapphire pulse laser with a pulse width of 130 fs and a repetition rate of 80 MHz. The excitation wavelength and the excitation power density were 800 nm and 1.2 nJ/cm^2, respectively.

III. RESULTS AND DISCUSSION

First, we discuss the morphology of the as-grown QDs on N-δ-doped GaAs. Figure 2 shows 1 × 1 μm^2 AFM images (left column) and histograms of the height (middle column) and aspect ratio (right column) of the QDs grown on (a) undoped GaAs and N-δ-doped GaAs with (b) $n_s = 1.7 \times 10^{12}$, (c) 8.5×10^{12}, and (d) 17×10^{12} cm^{-2}. Note that the giant dots formed by coalescence were excluded from the analysis. The QD height and aspect ratio for $n_s = 1.7 \times 10^{12}$ cm^{-2} exhibit unimodal distributions that approximately correspond to those for undoped GaAs. As the N-sheet density is increased, smaller QDs gradually appear and the bimodality of the distribution becomes pronounced, while the density of larger QDs decreases. Since the increase in the density of smaller QDs exceeds the decrease in the density of larger QDs, the total QD density at $n_s = 17 \times 10^{12}$ cm^{-2} is about 2.5-fold larger than that for undoped GaAs. The height of the larger QDs gradually decreases with increasing N-sheet density above $n_s = 1.7 \times 10^{12}$ cm^{-2}, while the base size remains almost constant. This leads to a smaller QD volume and a lower aspect ratio. Such a relationship between the aspect ratio and the QD volume has also been reported for QDs on undoped GaAs, in which the aspect ratio decreases with decreasing QD volume.[28,29] To discuss the factor causing the morphological variation in the QDs due to N-δ doping, the total QD volume was estimated as follows. First, we analyzed the [110], [-110] base sizes (not shown here) and height for each QD were analyzed in the area of 0.50 μm^2 for undoped GaAs and N-δ-doped GaAs with $n_s = 8.5 \times 10^{12}$ cm^{-2} and below and 0.75 μm^2 for $n_s = 17 \times 10^{12}$ cm^{-2}. The QD shape was assumed to be half-ellipsoid, in which the major and minor axes were the [110] and [-110] base sizes, respectively, and the volume of each QD was derived. Then, the total volume was derived by adding the volumes of all QDs in the observed area, which converted to the volume on 1 × 1 cm^2 area. The results for various N-sheet densities are shown in Fig. 3 (filled circles). The broken lines denote the values for the QDs on undoped GaAs. The total QD volume gradually decreases with increasing N-sheet density, while the wetting

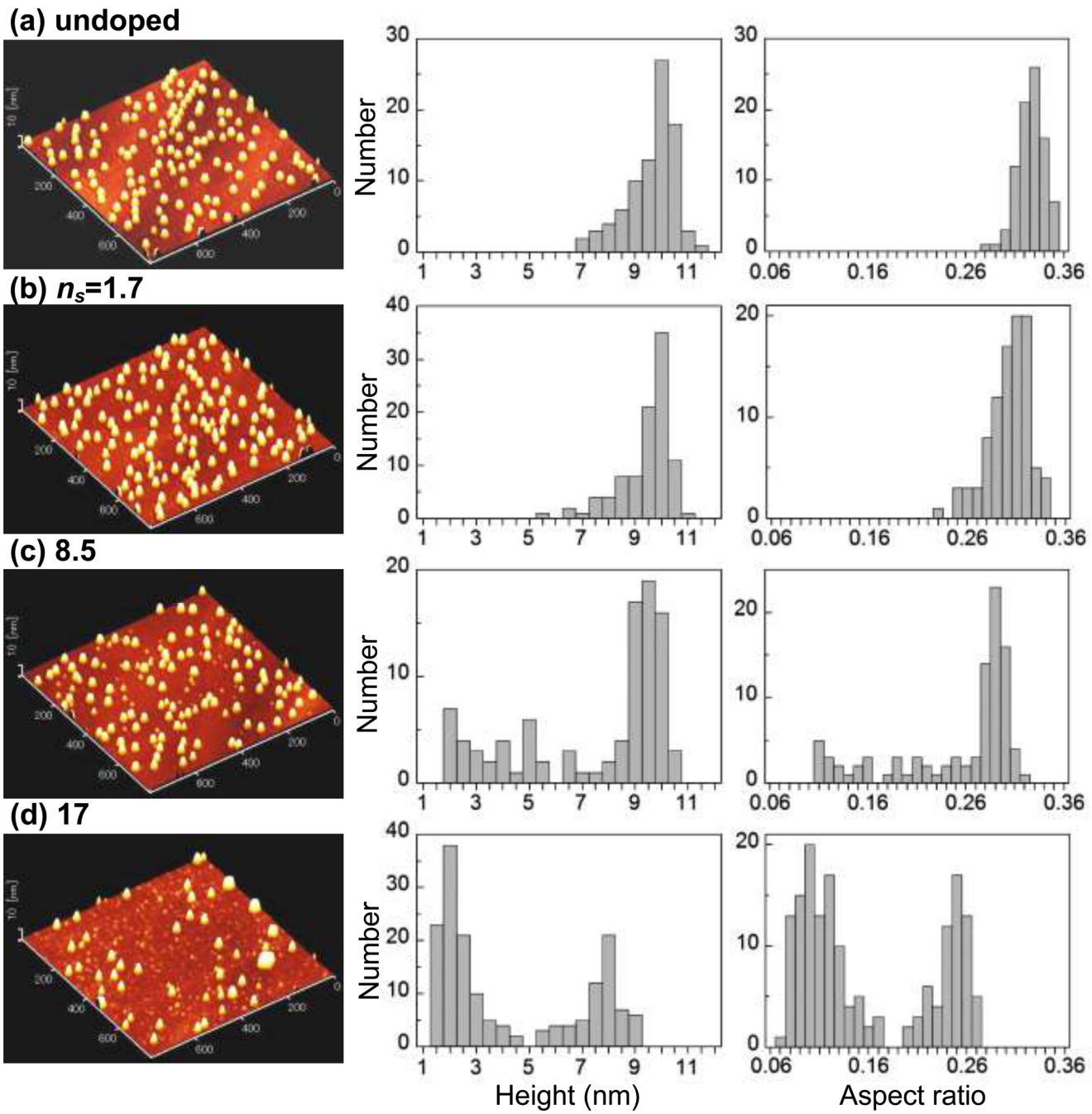

FIG. 2. $1 \times 1\ \mu m^2$ AFM images (left column) and histograms of the height (middle column) and aspect ratio (right column) of the QDs grown on (a) undoped GaAs and N-δ-doped GaAs with N-sheet densities of (b) $n_s = 1.7 \times 10^{12}$, (c) 8.5×10^{12}, and (d) $17 \times 10^{12}\,cm^{-2}$. The total QD densities are 1.9×10^{10}, 2.1×10^{10}, 1.9×10^{10}, and $4.9 \times 10^{10}\,cm^{-2}$ for undoped GaAs and N-δ-doped GaAs with $n_s = 1.7 \times 10^{12}$, 8.5×10^{12}, and $17 \times 10^{12}\,cm^{-2}$, respectively.

layer (WL) volume (open squares), estimated from the variation in the RHEED pattern due to the transition from two-dimensional (2D) growth to three-dimensional (3D) growth, is almost constant. Since the reevaporation of In atoms is negligible at the substrate temperature of 480 °C,[30] this result suggests that the incorporation of Ga and/or In atoms into the QDs from the underlying GaAs layer and/or WL occurs during the 3D growth on undoped GaAs and in the case of low-density N-δ doping, whereas it is suppressed in the case of high-density N-δ doping. A similar suppression effect of In-Ga intermixing has been reported for N-δ doping on a QD surface,[22–24] in which the intermixing between the QDs and the GaAs cap layer was suppressed because of large bonding energy of Ga-N or In-N (the bonding energies of Ga-N, In-N, Ga-As, and In-As are 2.24, 1.93, 1.63, and 1.55 eV, respectively).[31,32]

N-δ doping on the GaAs surface also affects the PL properties of the QDs. Figure 4 shows the room-temperature PL spectra of the QDs on undoped GaAs (broken line) and N-δ-doped GaAs with various N-sheet densities (solid lines). The spectra have a shoulder on the shorter-wavelength side of the main peak, which originates from the excited-state transition of the QDs for undoped GaAs and N-δ-doped GaAs with $n_s = 8.5 \times 10^{12}$ and below. On the other hand, the

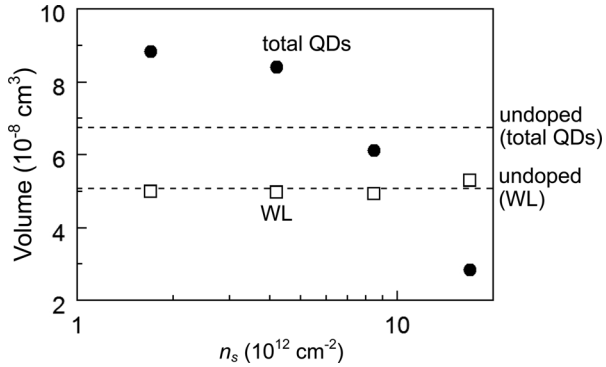

FIG. 3. Total QD volume (filled circles) and WL volume (open squares) as functions of the N-sheet density (n_s). The total QD volume was estimated from the QD density and size distribution. The WL volume was estimated from the variation in the RHEED pattern due to the transition from 2D to 3D growth. The broken lines denote the values for the QDs on undoped GaAs.

shoulder for $n_s = 17 \times 10^{12}\,\mathrm{cm}^{-2}$ is mainly due to the emission from the ground state of smaller QDs. Since smaller QDs tend to cause the thermal carrier escape, the PL spectrum exhibits a Gaussian shape with only a small shoulder at room temperature, despite a bimodal distribution of the as-grown QD size shown in Fig. 2(d). The peak wavelength is blueshifted with respect to that for undoped GaAs at the N-sheet densities of below $n_s = 8.5 \times 10^{12}\,\mathrm{cm}^{-2}$. As the N-sheet density is increased, the peak wavelength is monotonically redshifted and becomes longer than that for undoped GaAs at the N-sheet densities of $n_s = 8.5 \times 10^{12}\,\mathrm{cm}^{-2}$ and above. Thereby, tuning of the emission wavelength over about 80 nm is observed at room temperature. This behavior is opposite to the shift in the emission wavelength expected from the variation in the as-grown QD size, which implies that other factors, such as the size variation during capping and the composition of the QDs, affect the emission wavelength of the QDs. To analyze the QD morphology after GaAs capping in detail, we performed cross-sectional STEM observations. Figure 5 shows high-resolution (110) cross-sectional HAADF-STEM images of QDs grown on (a) undoped GaAs and N-δ-doped GaAs with (b) $n_s = 1.7 \times 10^{12}$, (c) 8.5×10^{12}, and (d) $17 \times 10^{12}\,\mathrm{cm}^{-2}$. We selected the largest QD from more than 10 cleaved QDs for each N-sheet density and derived the height, which is a reliable method for obtaining information on a QD cleaved near its center. The height of the embedded QDs is almost the same for all the N-sheet densities, whereas the height of the as-grown QDs decreases above $n_s = 1.7 \times 10^{12}\,\mathrm{cm}^{-2}$, as shown in Fig. 2. Since the large QDs are subjected to more lattice stain relaxation in as-grown than the small QDs, the strain due to lattice mismatch at the interface between the QDs and the GaAs cap layer is larger, which enhances the In-Ga intermixing and the In segregation during capping.[33] Therefore, the differences in the sizes of the embedded QDs among the different N-sheet densities are very small. Moreover, whereas a clear WL with about 2 ML thickness and an abrupt interface between the WL and the underlying GaAs layer is observed at a high N-sheet density, the WL morphology and the interface are unclear at a low N-sheet density. This suggests that the In-Ga intermixing between the WL and the underlying GaAs layer and the subsequent incorporation of Ga into the QDs are suppressed (enhanced) at a high (low) N-sheet density. This is consistent with the analysis results for the total QD volume shown in Fig. 3.

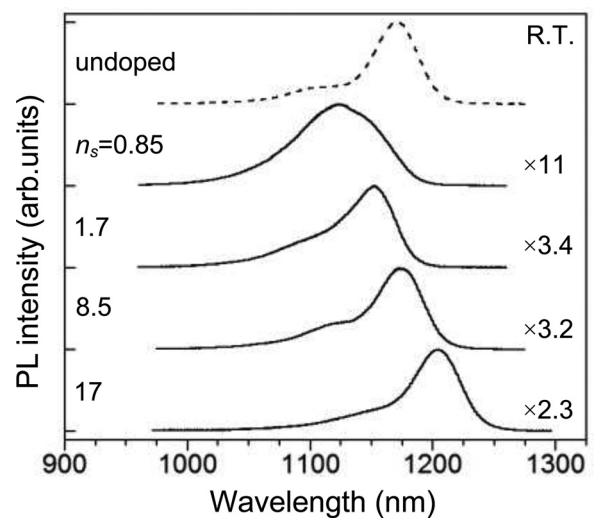

FIG. 4. Room-temperature PL spectra of the QDs on undoped GaAs (broken line) and N-δ-doped GaAs with various N-sheet densities (n_s) (solid lines).

Next, we investigated the composition of the QDs, which is another factor affecting the emission wavelength, from the measurement temperature dependence of the PL peak energy. Figure 6(a) shows the PL peak energy of the QDs as a function of the measurement temperature for undoped GaAs and N-δ-doped GaAs with various N-sheet densities. The solid lines represent the energy gap shrinkage of the QDs estimated from the Vina model, which is based on the Bose–Einstein statistical distribution for phonons[34]

$$E(T) = E(0) - \frac{A}{e^{\frac{\theta}{T}} - 1} = E(0) - \frac{A}{e^{\frac{\hbar\omega}{k_B T}} - 1}, \qquad (1)$$

where $E(0)$ is the energy gap at 0 K, A is the Vina coefficient, and θ is a material-specific phonon temperature, which represents the effective phonon energy $\hbar\omega = k_B\theta$, where k_B is the Boltzmann constant. The parameters were determined by fitting to the measured data in the low-temperature region below 120 K and the high-temperature region above 220 K. The PL peak energy exhibits a sigmoidal dependence on the measurement temperature, which is interpreted to originate from the thermally induced transfer of carriers from the QDs with higher ground state to those with lower ground state.[35,36] The bimodality of the distribution of the QD ground-state is more pronounced at a low N-sheet density, and thereby, the PL spectrum has a broad linewidth as shown in Fig. 4. The variation in the energy gap in semiconductors with respect to the measurement temperature is conventionally analyzed using the Varshni model[37]

$$E(T) = E(0) - \frac{\alpha T^2}{\beta + T}, \qquad (2)$$

where $E(0)$ is the energy gap at 0 K, and α and β are the Varshni coefficients. However, the Vina model sometimes

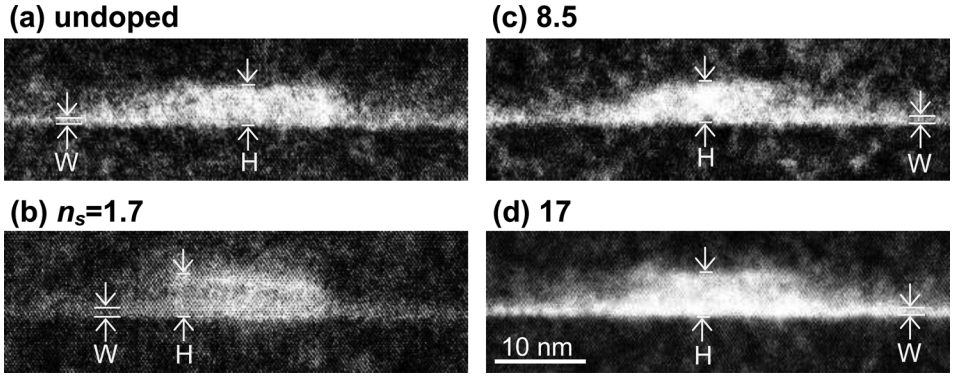

FIG. 5. High-resolution (110) cross-sectional HAADF-STEM images of the QDs grown on (a) undoped GaAs and N-δ-doped GaAs with N-sheet densities of (b) $n_s = 1.7 \times 10^{12}$, (c) 8.5×10^{12}, and (d) $17 \times 10^{12}\,\mathrm{cm}^{-2}$. The largest QD was selected from more than 10 cleaved QDs for each N-sheet density. The QD heights (H-W) are 3.6, 3.8, 3.8, and 3.8 nm for undoped GaAs and N-δ-doped GaAs with $n_s = 1.7 \times 10^{12}$, 8.5×10^{12}, and $17 \times 10^{12}\,\mathrm{cm}^{-2}$, respectively.

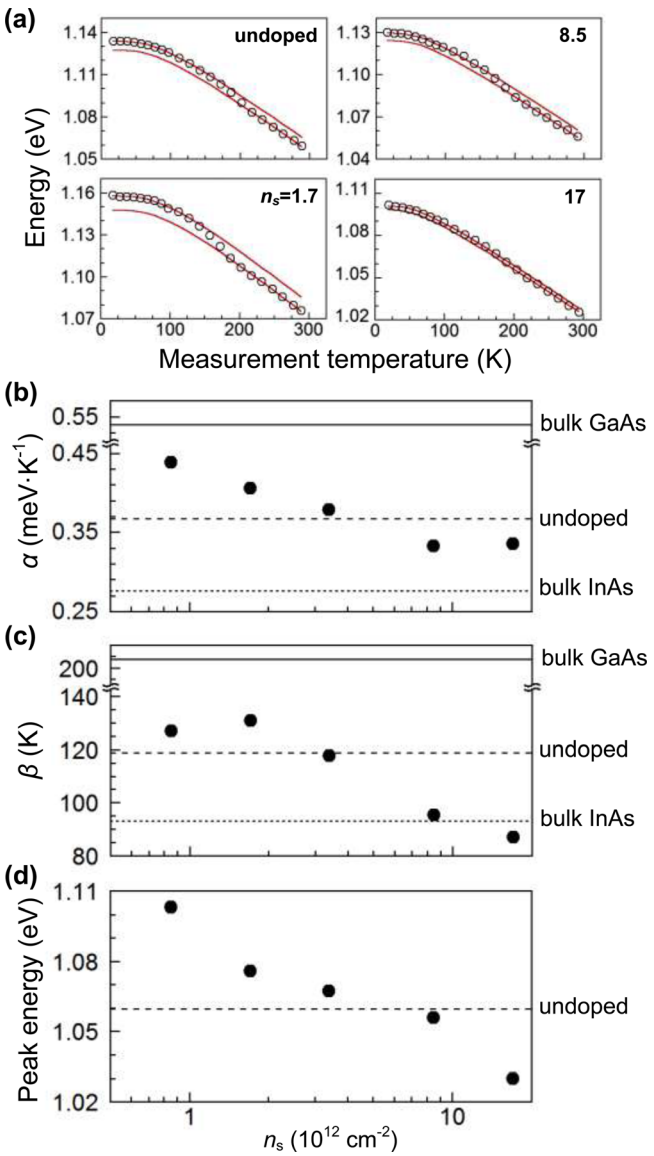

FIG. 6. (a) Measurement temperature dependence of the PL peak energy for various N-sheet densities (n_s). The solid lines represent the energy gap shrinkage of the QDs estimated from the Vina model. Varshni coefficients (b) α and (c) β as functions of n_s. The Varshni coefficients were derived using the Vina coefficients obtained by fitting the PL energy shift. The broken, solid, and dotted lines denote the values for the QDs on undoped GaAs, bulk GaAs, and bulk InAs, respectively. (d) PL peak energy of the QDs as a function of n_s. The broken line denotes the value for undoped GaAs.

gives better agreement with the PL energy shift in the low-temperature region than the Varshni model when the variation in the energy gap is affected by the electron-phonon interaction rather than by thermal expansion.[38,39] In contrast, in the high-temperature region, both models provide a good description of the PL energy shift. Note that the Varshni coefficients are related to the Vina coefficients as $\alpha = Ak_B/\hbar\omega$ and $\beta = \hbar\omega/2k_B$.[39] We derived the Varshni coefficients from the Vina coefficients obtained by fitting the PL energy shift in Fig. 6(a) for comparison with the values for bulk GaAs and InAs in the literature.[40] The results for various N-sheet densities are shown in Figs. 6(b) and 6(c). The broken, solid, and dotted lines denote the values for the QDs on undoped GaAs, bulk GaAs, and bulk InAs, respectively. The values of α and β are larger than those for undoped GaAs at the N-sheet densities of $n_s = 3.4 \times 10^{12}\,\mathrm{cm}^{-2}$ and below, which suggests the high Ga composition of the QDs. In contrast, the fact that α and β gradually approach the values for bulk InAs with increasing N-sheet density indicates an increase in the In composition. Since these behaviors of α and β correspond well to the N-sheet density dependence of the PL peak energy shown in Fig. 6(d), the variation in the composition of the QDs greatly affects the shift of the emission wavelength. The mechanism of the N-sheet density-dependent variation in the composition of the QDs is considered to be as follows. N-δ doping has two opposite and competing effects on the incorporation of Ga from the underlying layer into the QDs during the QD growth. One is the enhancement of Ga incorporation induced by the lattice strain. Since N atoms have a smaller radius than As atoms, more lattice strain is accumulated at the interface between the WL and the underlying GaAs layer, which enhances the In-Ga intermixing and the incorporation of Ga into the QDs.[41] The other is an effect blocking for Ga incorporation, which is due to the large bonding energy of Ga-N or In-N. At a low N-sheet density, the lattice-strain effect is dominant. Since the N atoms δ-doped are not uniformly distributed and spatially localized on the GaAs surfaces[42] when the N-sheet density approaches the QD density, the lattice strain caused by the smaller radius of N atoms fluctuates on the surface. Thereby, Ga incorporation from the underlying layer into the QDs also depends on the fluctuation, which results in the broad PL spectrum reflecting a bimodal composition distribution of QDs shown in Fig. 4. On the other hand, the blocking effect becomes larger with increasing N-sheet density and eventually exceeds the lattice-strain effect.

Therefore, the incorporation of Ga from the underlying layer depends on the N-sheet density. Since the In-Ga intermixing between the QDs and the GaAs cap layer during capping also depends on the N-sheet density, which is enhanced (suppressed) at a low (high) N-sheet density owing to the large (small) QD size in as-grown, the composition of the QDs is determined by the superposition of three factors: Ga incorporation from the underlying layer induced by the lattice strain, which is promoted by N-δ doping, the blocking of Ga incorporation by the N-δ doping layer, and the intermixing between the QDs and the cap layer. Note that few N atoms are considered to be incorporated into the QDs because the marked decrease in α and β reported for InAsN QDs[23] was not observed even at a high N-sheet density. To investigate the effect of the enhancement of lattice strain caused by N-δ doping, we fabricated a QD sample in which a thin GaAs spacer layer was introduced between the N-δ doping layer and the WL. Figure 7 shows the room-temperature PL spectra of the QDs grown on N-δ-doped GaAs with and without the GaAs spacer layer. The N-sheet densities of both samples are $n_s = 17 \times 10^{12}\,\mathrm{cm}^{-2}$. The spacer thickness is 1 nm. The PL spectrum for undoped GaAs is also shown for reference (broken line). Whereas the peak wavelength for the QDs without a spacer layer exhibits a redshift with respect to that for undoped GaAs, the peak wavelength for the QDs with a spacer layer exhibits a blueshift comparable to that for the lowest N-sheet density of $n_s = 0.85 \times 10^{12}\,\mathrm{cm}^{-2}$ shown in Fig. 4. In addition, the Varshni coefficients α and β estimated from the measurement temperature dependence of the PL peak energy were $0.41\,\mathrm{meV \cdot K^{-1}}$ and 165 K, respectively, which are also comparable to those for the lowest N-sheet density shown in Figs. 6(b) and 6(c). Since the spacer layer is subjected to compressive strain from the N-δ doping layer, large lattice strain is accumulated at the interface between the WL and the spacer layer. Therefore, these results support the speculation that N-δ doping has not only the effect blocking for Ga incorporation but also the promotion effect of the lattice-strain-induced incorporation of Ga atoms.

To further investigate the effect of N-δ doping on the optical properties of the QDs, we performed time-resolved PL measurements. Figure 8(a) shows typical PL decay profiles of the QDs for undoped GaAs and N-δ-doped GaAs with various N-sheet densities, which were recorded at the peak wavelength of the ground-state emission from the QDs. The measurement temperature was 3.4 K. All the profiles can be fitted by a single exponential function. The recombination lifetime of the QD excitons (τ) derived from these profiles are 1.0, 1.2, 1.5, and 1.5 ns for undoped GaAs, $n_s = 1.7 \times 10^{12}$, 8.5×10^{12}, and $17 \times 10^{12}\,\mathrm{cm}^{-2}$, respectively. τ is inversely proportional to the oscillator strength, given by the electronic dipole transition and the overlap integral of the electron and hole wavefunctions.[43] Since the oscillator strength depends on the emission wavelength, which is related to the QD size, the detection wavelength dependence of τ for each sample was measured. The results are summarized in Fig. 8(b). The analyzed range of wavelengths was the full width at quarter maximum of the time-integrated PL spectrum, in which the decay profiles exhibited a high signal-to-noise ratio. A filled mark denotes the value at the peak wavelength for each sample. A clear dependence on the N-sheet density as τ increases with the N-sheet density was observed. This suggests that the lattice strain that accumulated in the QDs due to the high-density N-δ doping and the associated high In composition induces the piezoelectric

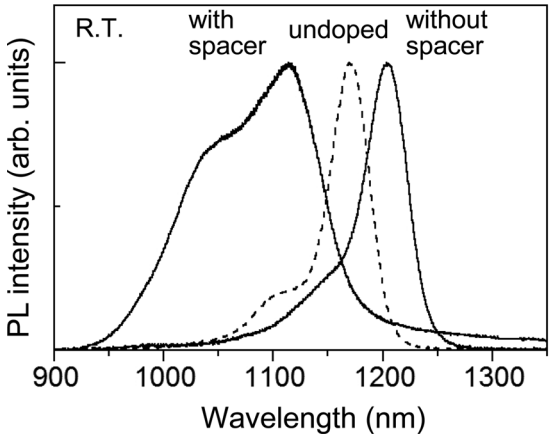

FIG. 7. Room-temperature PL spectra of the QDs grown on N-δ-doped GaAs with and without the GaAs spacer layer. The N-sheet densities of both samples are $n_s = 17 \times 10^{12}\,\mathrm{cm}^{-2}$. The spacer thickness is 1 nm. The broken line denotes the PL spectrum for undoped GaAs for reference.

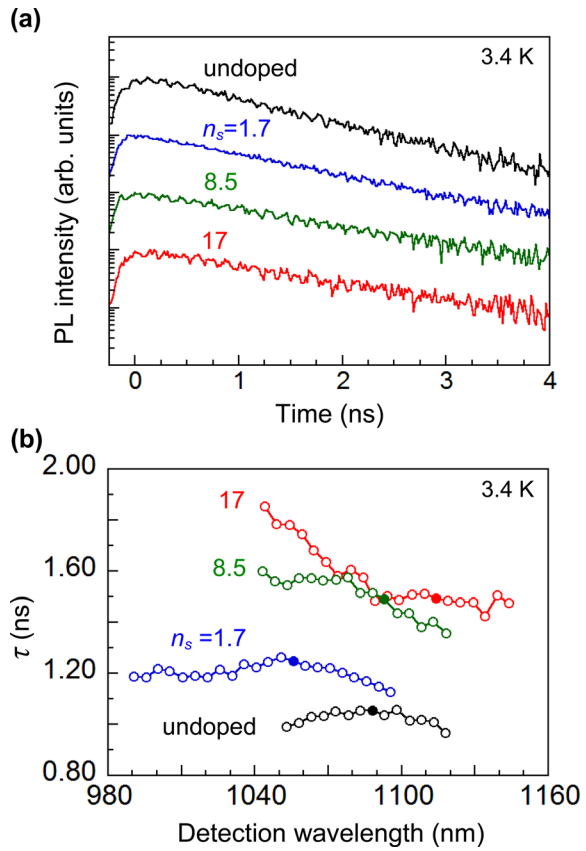

FIG. 8. (a) PL decay profiles of the QDs for undoped GaAs and N-δ-doped GaAs with various N-sheet densities, which were recorded at the peak wavelength of the ground-state emission from the QDs. (b) Detection wavelength dependence of the recombination lifetime (τ) of the QD excitons for undoped GaAs and N-δ-doped GaAs with various N-sheet densities. The analyzed range of wavelength was the full width at quarter maximum of the time-integrated PL spectrum. A filled mark denotes the value at the peak wavelength for each sample. The measurement temperature was 3.4 K.

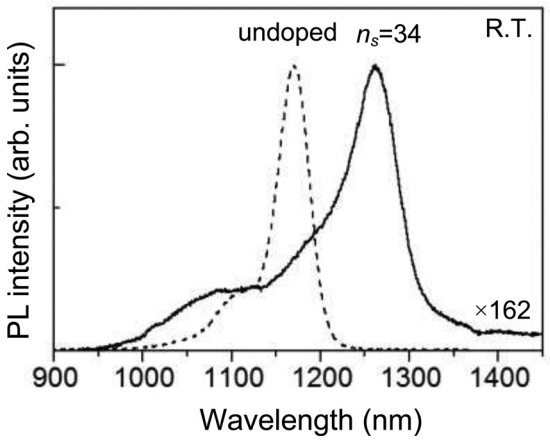

FIG. 9. Room-temperature PL spectrum of the QDs grown on N-δ-doped GaAs with a N-sheet density of $n_s = 34 \times 10^{12}\,\mathrm{cm}^{-2}$. The broken line denotes the PL spectrum for undoped GaAs for reference.

effect, and thereby the overlap integral of the electron and hole wavefunctions decreases,[44] which simultaneously induces a redshift of the emission wavelength.[45] In addition, a marked increase in τ at the detection wavelength shorter than about 1070 nm for $n_s = 17 \times 10^{12}\,\mathrm{cm}^{-2}$, at which the emission from the ground state of smaller QDs in Fig. 2(d) is dominant, is also attributed to the piezoelectric effect. From the discussion in Fig. 3, it is deduced that the N-sheet density has a local distribution and smaller QDs are formed on the GaAs surface with high N-sheet density. Thereby, the enhanced piezoelectric effect leads to a longer recombination lifetime.

Finally, we demonstrate the extension of the emission wavelength towards the longer-wavelength region by higher-density N-δ doping. Figure 9 shows the room-temperature PL spectrum of the QDs grown on N-δ-doped GaAs with a N-sheet density of $n_s = 34 \times 10^{12}\,\mathrm{cm}^{-2}$. The PL spectrum for undoped GaAs is also shown for reference (broken line). The PL spectrum for N-δ doping exhibits emission at 1.26 μm, which almost coincides with the 1.3 μm optical communication band. The Varshni coefficients α and β estimated from the measurement temperature dependence of the PL peak energy were 0.31 meV K^{-1} and 92 K, respectively, which are comparable to those for the N-sheet densities of $n_s = 8.5 \times 10^{12}$ and $17 \times 10^{12}\,\mathrm{cm}^{-2}$ shown in Figs. 6(b) and 6(c). The fact that a marked decrease in α and β is not observed suggests little incorporation of N into the QDs. Therefore, the high In composition and the enhanced piezoelectric effect cause the long-wavelength emission. On the other hand, the PL intensity is significantly less than that for undoped GaAs, which is attributed to the crystal defects generated by excess N atoms in addition to the decreases in the QD density and recombination rate. It is expected to be possible to simultaneously attain a long-wavelength emission and a high emission intensity by further adjusting the N-δ doping conditions.

IV. SUMMARY

We studied the structural and PL characteristics of InAs QDs grown on N-δ-doped GaAs(001). The PL peak wavelength for a N-sheet density of $n_s = 3.4 \times 10^{12}\,\mathrm{cm}^{-2}$ and below was blueshifted with respect to that for undoped GaAs. As the N-sheet density was increased, the peak wavelength was monotonically redshifted and became longer than that for undoped GaAs above $n_s = 3.4 \times 10^{12}\,\mathrm{cm}^{-2}$. Thereby, tuning of the emission wavelength from 1.12 to 1.26 μm was achieved at room temperature. The emission wavelength was greatly affected by the variation in the In composition of the QDs. N-δ doping has two opposite and competing effects on the incorporation of Ga atoms from the underlying layer into the QDs during the QD growth. One is the enhancement of Ga incorporation induced by the lattice strain, which is due to the smaller radius of N atoms. The other is an effect blocking for Ga incorporation, which is due to the large bonding energy of Ga-N or In-N. At a low N-sheet density, the lattice-strain effect was dominant, while the blocking effect was dominant at a high N-sheet density. Therefore, the incorporation of Ga from the underlying layer depended on the N-sheet density. Since the In-Ga intermixing between the QDs and the GaAs cap layer during capping also depended on the N-sheet density, the superposition of these three factors determined the composition of the QDs. In addition, the increased lattice strain due to the high-density N-δ doping and the associated high In composition induced the piezoelectric effect, which also affected the PL properties of the QDs.

[1]Y. Arakawa and H. Sakaki, Appl. Phys. Lett. **40**, 939 (1982).
[2]D. Bimberg, M. Grundmann, and N. N. Ledentsov, *Quantum Dot Heterostructures* (Wiley, New York, 1998).
[3]H. Shoji, *Semiconductors and Semimetals* (Academic, San Diego, 1999), Vol. 60.
[4]M. Sugawara, N. Hatori, T. Akiyama, Y. Nakata, and H. Ishikawa, Jpn. J. Appl. Phys., Part 2 **40**, L488 (2001).
[5]T. Kita, O. Wada, H. Ebe, Y. Nakata, and M. Sugawara, Jpn. J. Appl. Phys., Part 2 **41**, L1143 (2002).
[6]P. Jayavel, H. Tanaka, T. Kita, O. Wada, H. Ebe, M. Sugawara, J. Tatebayashi, Y. Arakawa, Y. Nakata, and T. Akiyama, Appl. Phys. Lett. **84**, 1820 (2004).
[7]T. Kita, N. Tamura, O. Wada, M. Sugawara, Y. Nakata, H. Ebe, and Y. Arakawa, Appl. Phys. Lett. **88**, 211106 (2006).
[8]T. Inoue, M. Asada, N. Yasuoka, O. Kojima, T. Kita, and O. Wada, Appl. Phys. Lett. **96**, 211906 (2010).
[9]T. Kita, M. Suwa, T. Kaizu, and Y. Harada, J. Appl. Phys. **115**, 233512 (2014).
[10]T. Passow, S. Li, P. Feinäugle, T. Vallaitis, J. Leuthold, D. Litvinov, D. Gerthsen, and M. Hetterich, J. Appl. Phys. **102**, 073511 (2007).
[11]K. Nishi, H. Saito, S. Sugou, and J. S. Lee, Appl. Phys. Lett. **74**, 1111 (1999).
[12]N. Ozaki, T. Yasuda, S. Ohkouchi, E. Watanabe, N. Ikeda, Y. Sugimoto, and R. A. Hogg, Jpn. J. Appl. Phys., Part 1 **53**, 04EG10 (2014).
[13]Z. R. Wasilewski, S. Fafard, and J. P. McCaffrey, J. Cryst. Growth **201–202**, 1131 (1999).
[14]Y. Hino, N. Ozaki, S. Ohkouchi, N. Ikeda, and Y. Sugimoto, J. Cryst. Growth **378**, 501 (2013).
[15]Q. Gong, P. Offermans, R. Nötzel, P. M. Koenraad, and J. H. Wolter, Appl. Phys. Lett. **85**, 5697 (2004).
[16]H. Eisele, A. Lenz, R. Heitz, R. Timm, M. Dähne, Y. Temko, T. Suzuki, and K. Jacobi, J. Appl. Phys. **104**, 124301 (2008).
[17]I. Kegel, T. H. Metzger, A. Lorke, J. Peisl, J. Stangl, G. Bauer, and K. Nordlund, Phys. Rev. B **63**, 035318 (2001).
[18]T. Kaizu, M. Takahasi, K. Yamaguchi, and J. Mizuki, J. Cryst. Growth **301–302**, 248 (2007).
[19]T. Walther, A. G. Cullis, D. J. Norris, and M. Hopkinson, Phys. Rev. Lett. **86**, 2381 (2001).
[20]F. Ferdos, S. Wang, Y. Wei, A. Larsson, M. Sadeghi, and Q. Zhao, Appl. Phys. Lett. **81**, 1195 (2002).

[21]T. Kaizu, T. Matsumura, and T. Kita, J. Appl. Phys. **118**, 154301 (2015).
[22]T. Kita, T. Mori, M. Matsushita, M. Kikuno, O. Wada, H. Ebe, M. Sugawara, Y. Arakawa, and Y. Nakata, J. Appl. Phys. **97**, 024306 (2005).
[23]H. Mizuno, T. Inoue, M. Kikuno, T. Kita, O. Wada, H. Mori, and H. Yasuda, J. Cryst. Growth **301–302**, 709 (2007).
[24]T. Inoue, S. Kido, K. Sasayama, T. Kita, and O. Wada, J. Appl. Phys. **104**, 103532 (2008).
[25]P. B. Joyce, T. J. Krzyzewski, G. R. Bell, B. A. Joyce, and T. S. Jones, Phys. Rev. B **58**, R15981 (1998).
[26]T. Kita and O. Wada, Phys. Rev. B **74**, 035213 (2006).
[27]N. Shimizu, T. Inoue, T. Kita, and O. Wada, J. Cryst. Growth **301–302**, 34 (2007).
[28]F. M. Ross, J. Tersoff, and R. M. Tromp, Phys. Rev. Lett. **80**, 984 (1998).
[29]L. G. Wang, P. Kratzer, N. Moll, and M. Scheffler, Phys. Rev. B **62**, 1897 (2000).
[30]A. M. Ceschin and J. Massies, J. Cryst. Growth **114**, 693 (1991).
[31]X. Kong, A. Trampert, E. Tournié, and K. H. Ploog, Appl. Phys. Lett. **87**, 171901 (2005).
[32]W. A. Harrison, *Electronic Structure and the Properties of Solids* (Dover, New York, 1989), pp. 175–176.
[33]K. Yamaguchi, Y. Saito, and R. Ohtsubo, Appl. Surf. Sci. **190**, 212 (2002).
[34]L. Viña, S. Logothetidis, and M. Cardona, Phys. Rev. B **30**, 1979 (1984).
[35]R. Heitz, I. Mukhametzhanov, A. Madhukar, A. Hoffmann, and D. Bimberg, J. Electron. Mater. **28**, 520 (1999).
[36]H. Kissel, U. Müller, C. Walther, W. T. Masselink, Y. I. Mazur, G. G. Tarasov, and M. P. Lisitsa, Phys. Rev. B **62**, 7213 (2000).
[37]Y. P. Varshni, Physica **34**, 149 (1967).
[38]H. Khmissi, M. Baira, L. Sfaxi, L. Bouzaïene, F. Saidi, C. B. Chevallier, and H. Maaref, J. Appl. Phys. **109**, 054316 (2011).
[39]I. Yeo, J. D. Song, and J. Lee, Appl. Phys. Lett. **99**, 151909 (2011).
[40]I. Vurgaftman, J. R. Meyer, and L. R. Ram-Mohan, J. Appl. Phys. **89**, 5815 (2001).
[41]H. Y. Liu, M. Hopkinson, C. N. Harrison, J. Steer, and R. Frith, J. Appl. Phys. **93**, 2931 (2003).
[42]Y. Harada, M. Yamamoto, T. Baba, and T. Kita, Appl. Phys. Lett. **104**, 041907 (2014).
[43]U. E. H. Laheld and G. T. Einevoll, Phys. Rev. B **55**, 5184 (1997).
[44]G. Bester, A. Zunger, X. Wu, and D. Vanderbilt, Phys. Rev. B **74**, 081305 (2006).
[45]S. S. Li and J. B. Xia, J. Appl. Phys. **88**, 7171 (2000).